

Figure 5.13. Temporal and spatial dynamics of potential breeding sites for the red-billed quelea (*Quelea quelea*) over East Africa as computed from information obtained from the AVHRR sensor on board the NOAA satellites. Season is noted on each image. Maps from Wallin (1990).

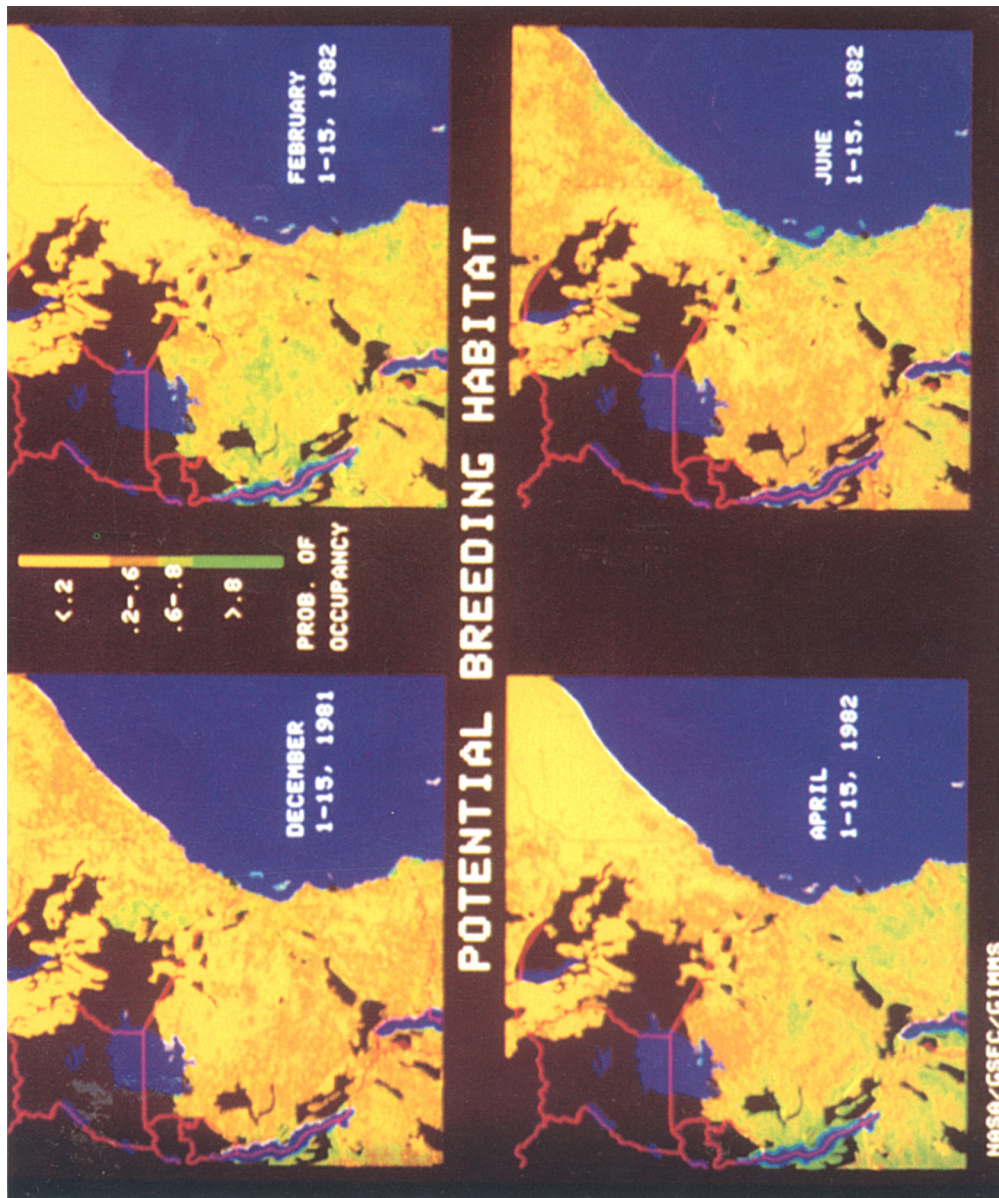
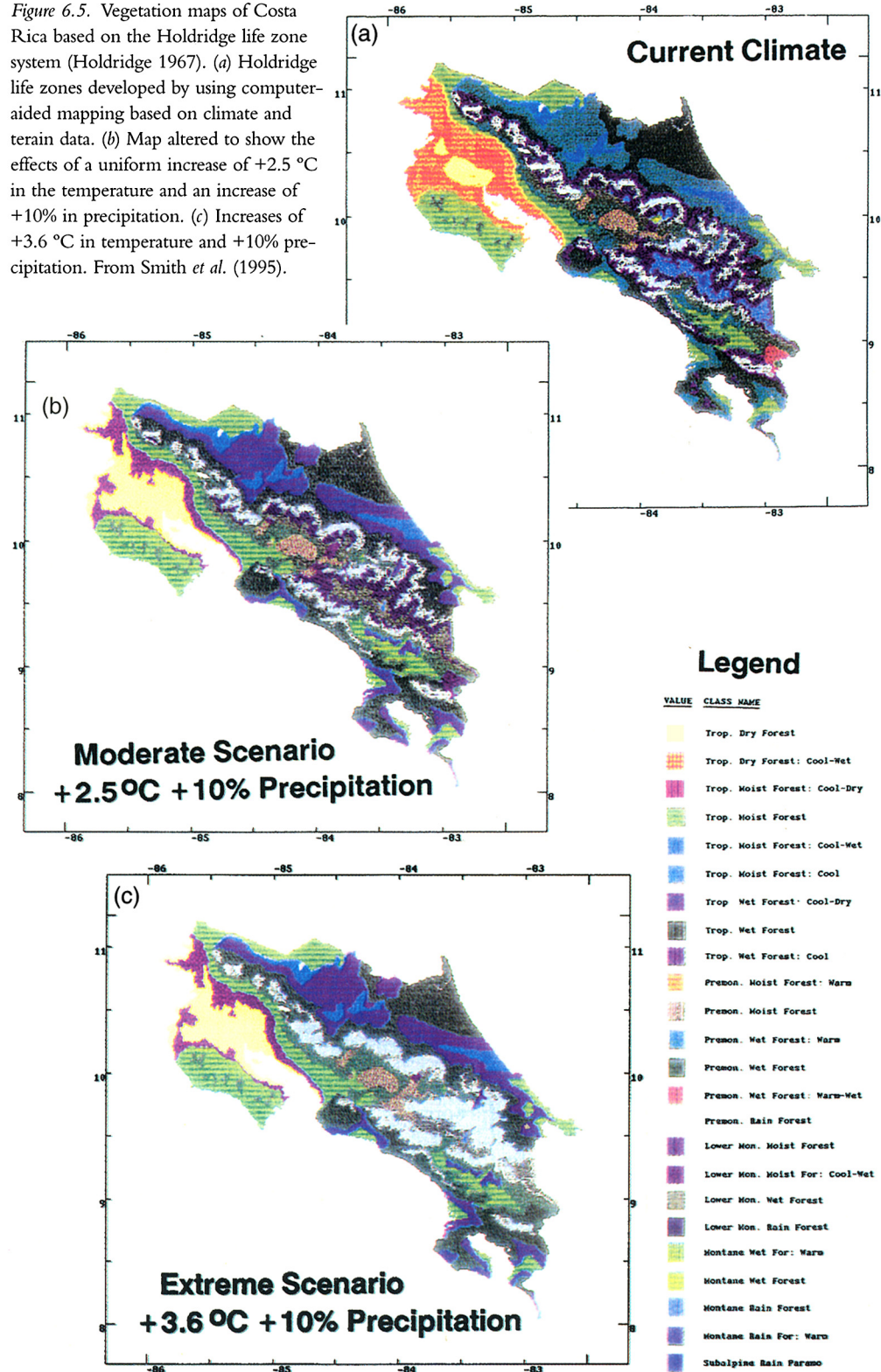
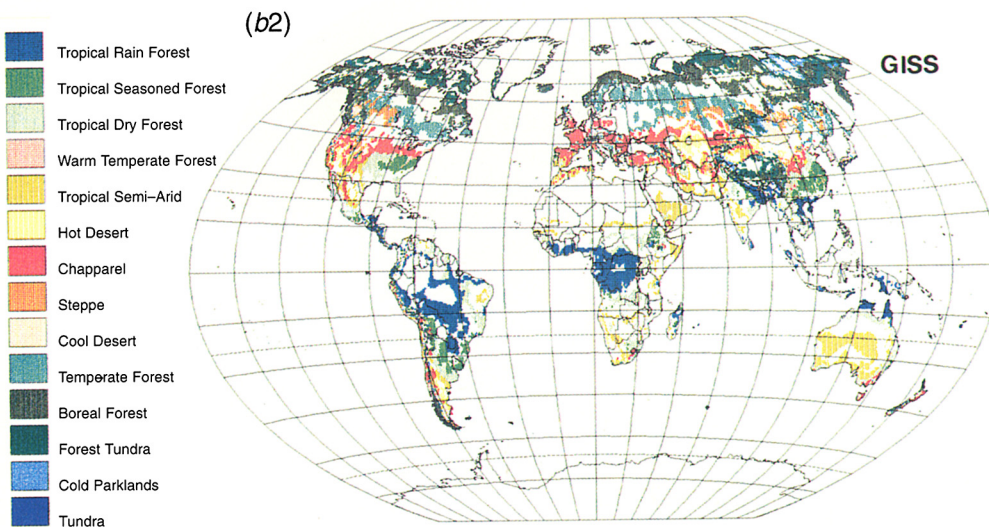
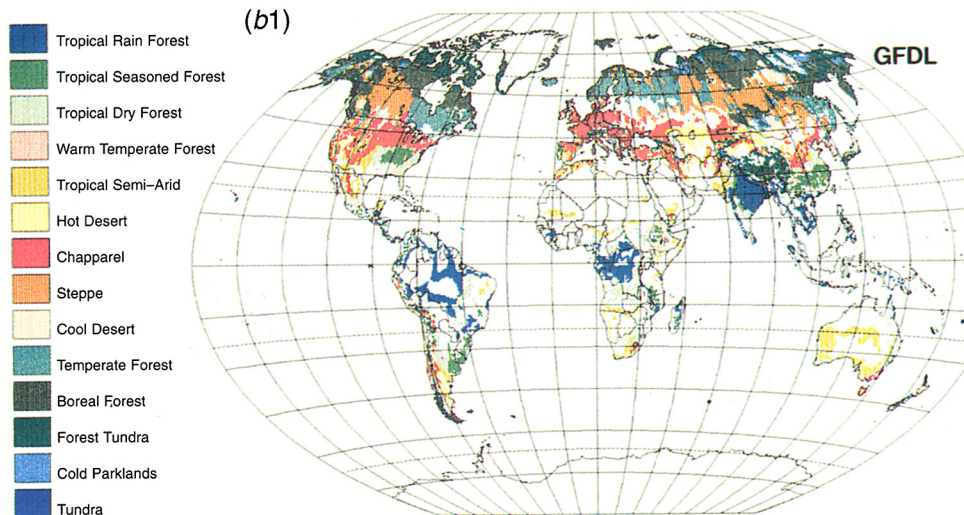
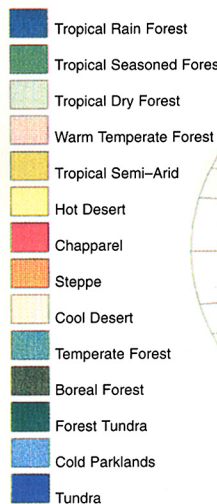


Figure 6.5. Vegetation maps of Costa Rica based on the Holdridge life zone system (Holdridge 1967). (a) Holdridge life zones developed by using computer-aided mapping based on climate and terrain data. (b) Map altered to show the effects of a uniform increase of +2.5 °C in the temperature and an increase of +10% in precipitation. (c) Increases of +3.6 °C in temperature and +10% precipitation. From Smith *et al.* (1995).





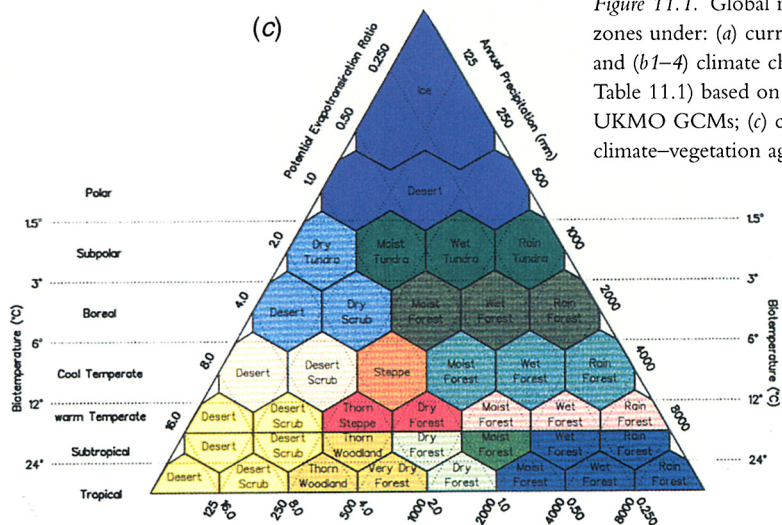
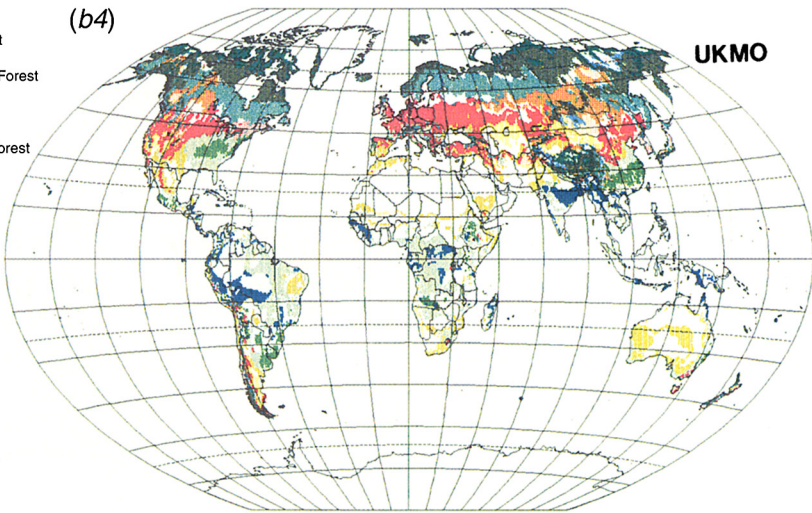
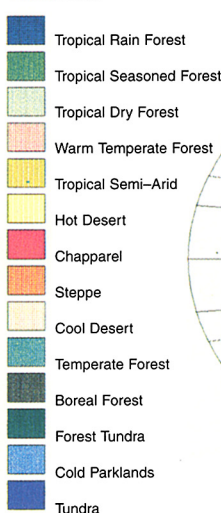
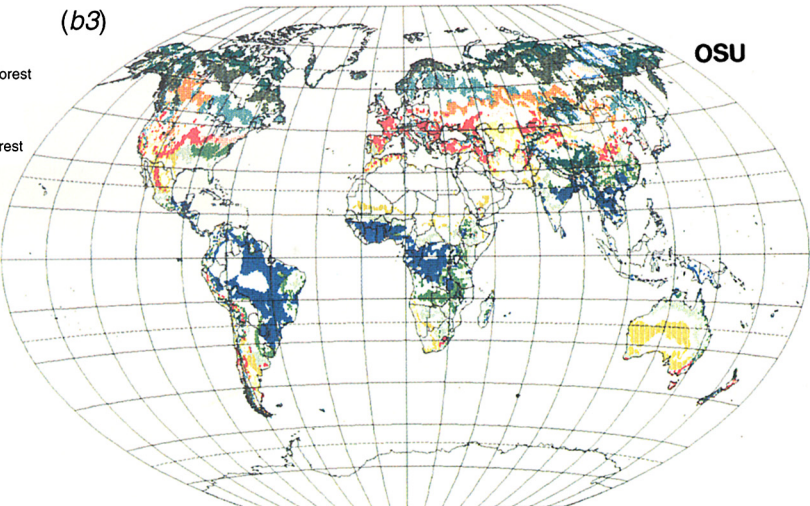
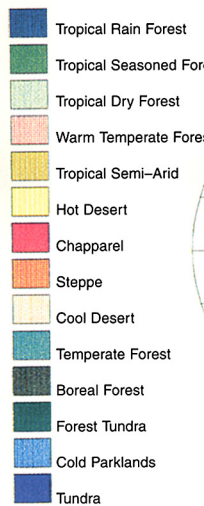


Figure 11.1. Global map of Holdridge life zones under: (a) current climate conditions and (b1–4) climate change scenarios (see Table 11.1) based on GFDL, GISS, OSU, UKMO GCMs; (c) colour key to Holdridge climate–vegetation aggregation scheme.

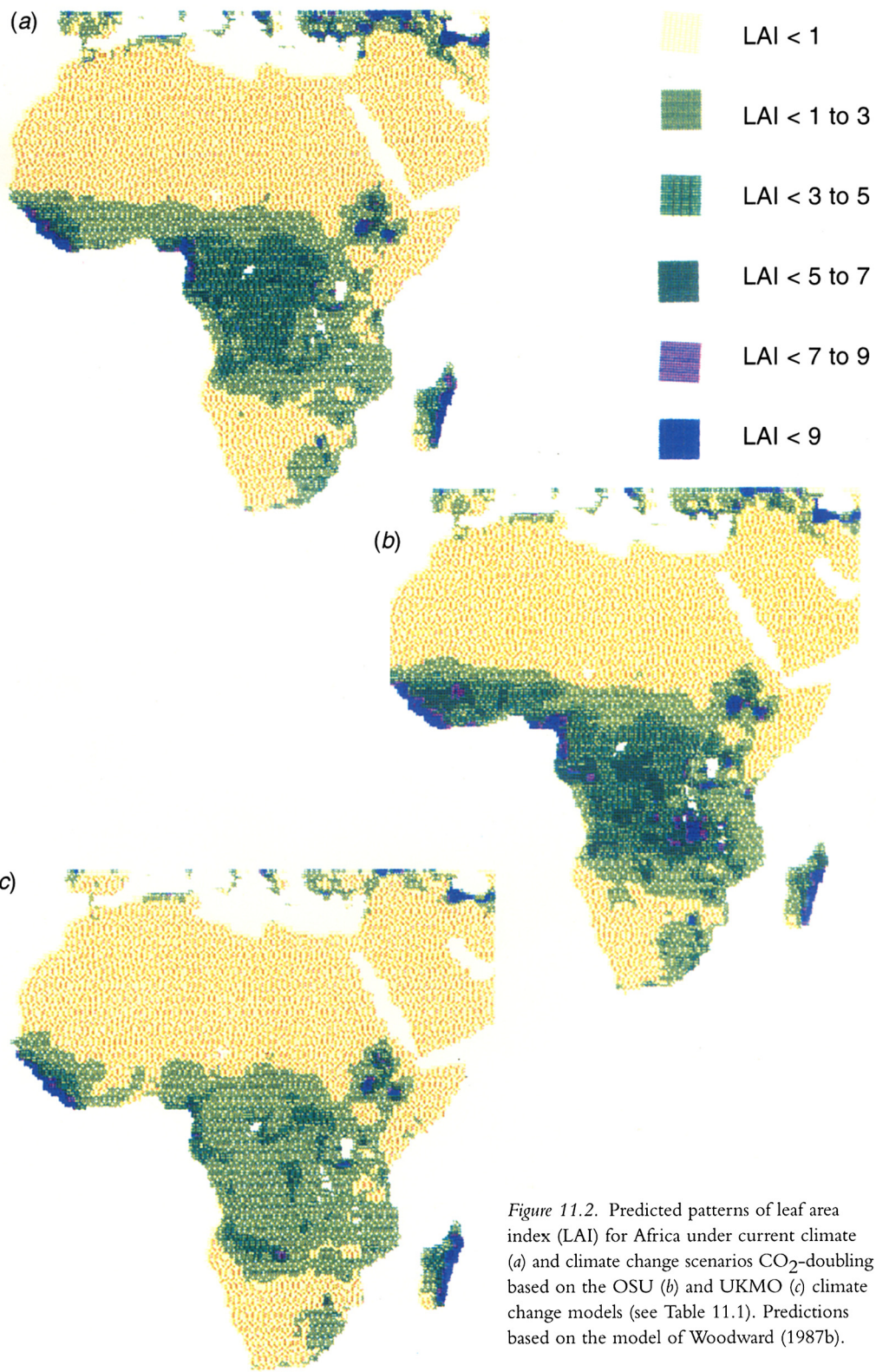


Figure 11.2. Predicted patterns of leaf area index (LAI) for Africa under current climate (a) and climate change scenarios CO₂-doubling based on the OSU (b) and UKMO (c) climate change models (see Table 11.1). Predictions based on the model of Woodward (1987b).

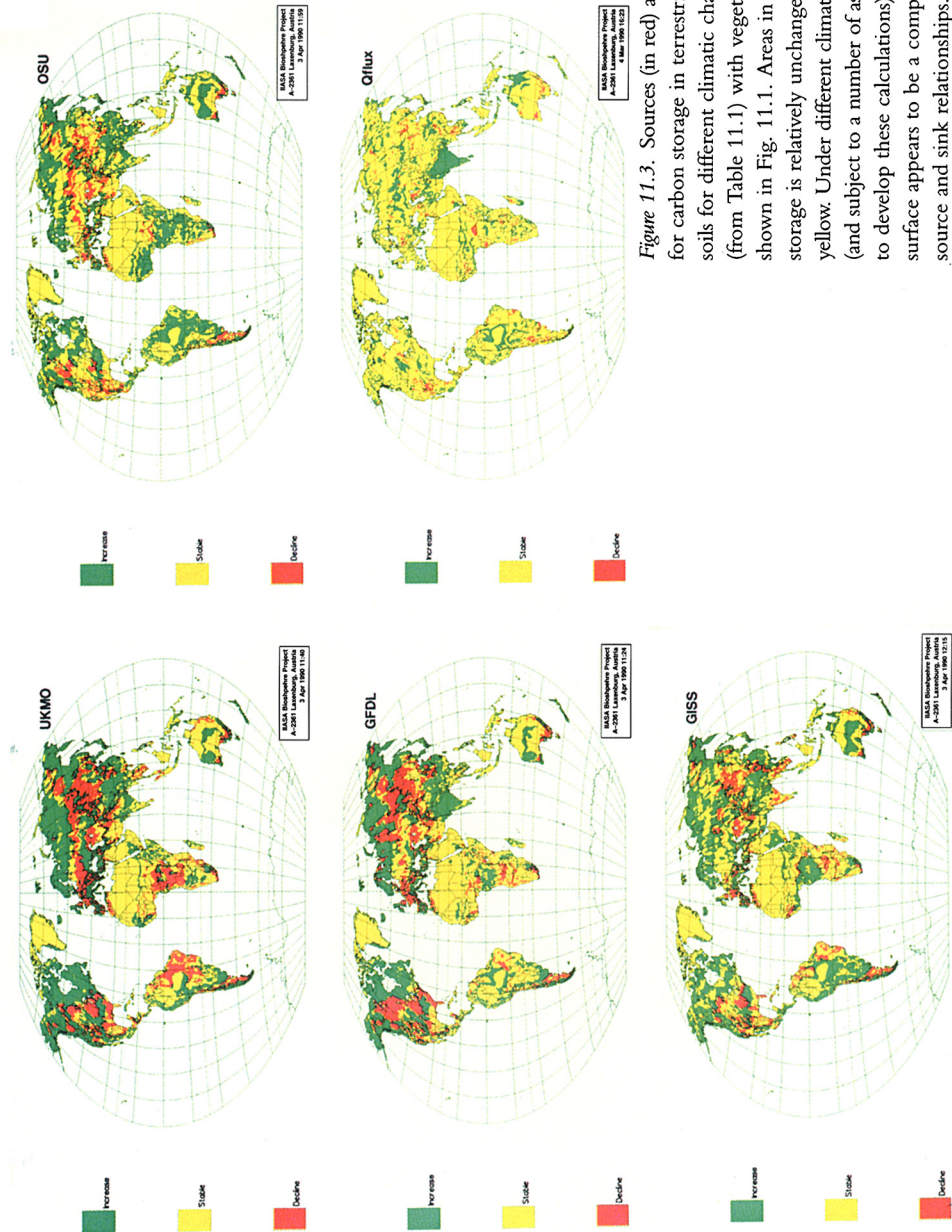


Figure 11.3. Sources (in red) and sinks (in green) for carbon storage in terrestrial vegetation and soils for different climatic change scenarios (from Table 11.1) with vegetation changes shown in Fig. 11.1. Areas in which the carbon storage is relatively unchanged are shown in yellow. Under different climate change scenarios (and subject to a number of assumptions needed to develop these calculations), the terrestrial surface appears to be a complex array of source and sink relationships.

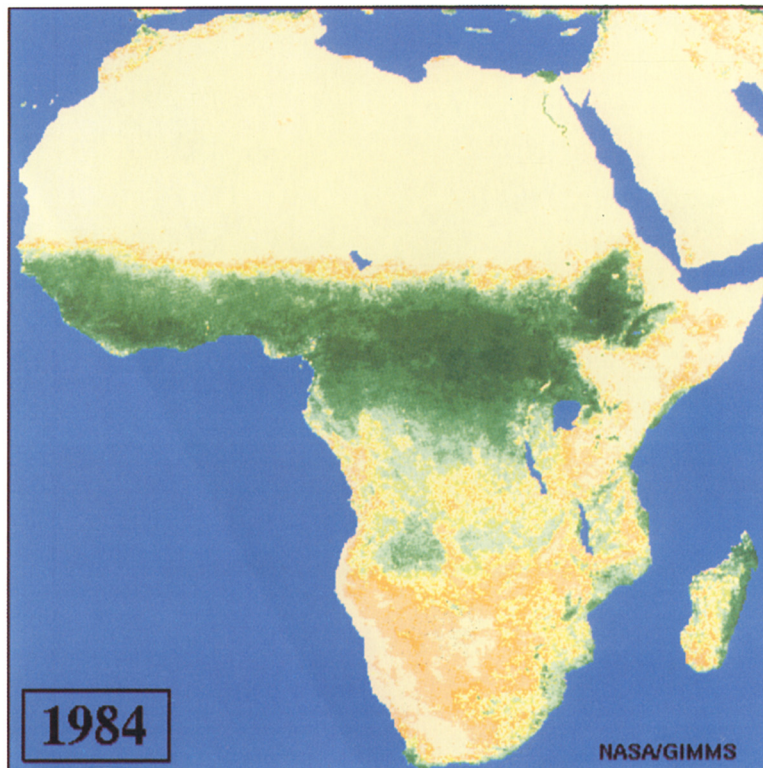
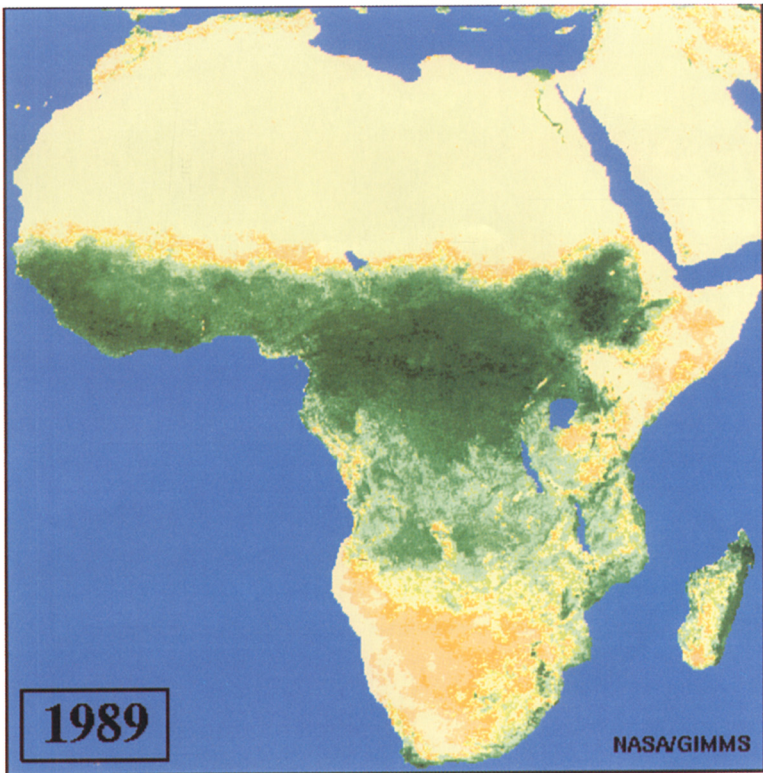


Figure 12.5. Shifts in the vegetation greenness on the Sahelian zone in 1984 and 1989 as detected by the NDVI of 'greenness' using the visible red and the near-infrared channels of the NOAA-7 satellite.
Images from C. J. Tucker and J. Kendall.

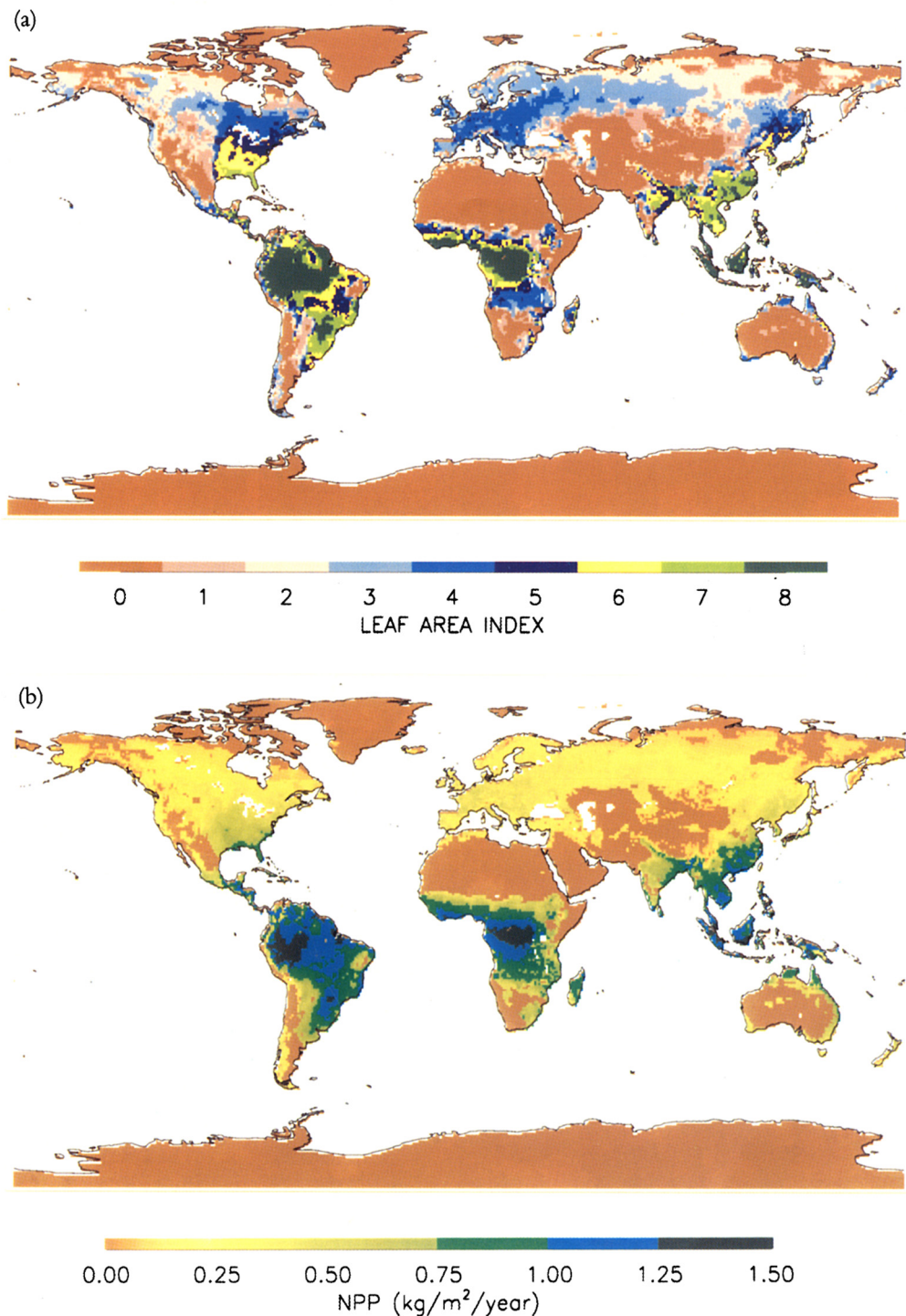


Figure 13.6. (a) Global distribution of leaf area index as predicted by the DOLY model of Woodward *et al.* (1995). (b) Global pattern of net annual productivity as produced by the DOLY model.